Article

Introducing Novel Redox-Active Bis(phenolate) N-Heterocyclic Carbene Proligands: Investigation of Their Coordination to Fe(II)/Fe(III) and Their Catalytic Activity in Transfer Hydrogenation of Carbonyl Compounds

Abdollah Neshat,* Ali Mousavizadeh Mobarakeh, Mohammad Reza Yousefshahi, Fahimeh Varmaghani, Michal Dusek, Vaclav Eigner, and Monika Kucerakova

Read Online

ACCESS | Metrics & More | Article Recommendations | SI Supporting Information

ABSTRACT: A simple and efficient procedure for synthesizing novel pincer-type tridentate N-heterocyclic carbene bisphenolate ligands is reported. The synthesis of pincer proligands with N,N′-disubstituted imidazoline core, **5** and **6**, was carried out via triethylorthoformate-promoted cyclization of either N,N′-bis(2-hydroxy-3,5-di-tert-butylphenyl)cyclohexanediamine, **3**, or N,N′-bis(2-hydroxyphenyl)cyclohexanediamine, **4**, in the presence of concentrated hydrochloric acid. Cyclic voltammograms of the ligands revealed ligand-centered redox activity, indicating the noninnocent nature of the ligands. The voltammograms of the ligands exhibit two successive one-electron oxidations and two consecutive one-electron reductions. In contrast to previous reports, the redox-active ligands in this study exhibit one-electron oxidation and reduction processes. All products were thoroughly characterized by using ^1H and ^{13}C NMR spectroscopy. The base-promoted deprotonation of the proligands and subsequent reaction with iron(II) and iron(III) chlorides yielded compounds **7** and **8**. These compounds are binuclear and tetranuclear iron(III) complexes that do not contain carbene functional groups. Complexes **7** and **8** were characterized by using elemental analysis and single-crystal X-ray crystallography. At low catalyst loadings, both **7** and **8** exhibited high catalytic activity in the transfer hydrogenation of selected aldehydes and ketones.

Novel Redox Active Ligands

☑ Synthesis and Characterization of Fe(III) Complexes
☑ Catalytic Transfer Hydrogenation Reactions
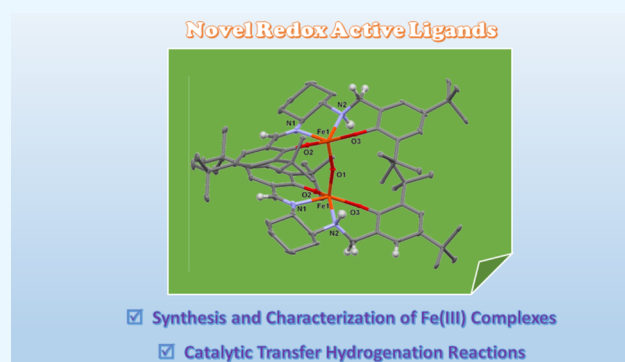
INTRODUCTION

Since its introduction in 1976 by Shaw, pincer ligands have become an important class of ligands in modern coordination and organometallic chemistry.[1−10] One outstanding feature of a pincer ligand is its σ-coordination along with two coplanar neutral or anionic side donations, often instilling stability in the resulting metal complexes and forming well-defined structural motifs. These novel structural motifs could be particularly interesting from catalytic activity viewpoints. Strong chelating features of pincer ligands coupled with redox activity could, in principle, bring about nobility to the electronic properties of the whole metal complex. This is particularly interesting when we consider the high cost of noble metal catalysis and the fact that there are still catalytic transformations that are limited in scope and require more potent noble or base metal catalysts for practical uses. In this regard, metal complexes employing redox-active ligands represent a growing field in catalytic reactions. These ligands could act similarly to multifunctional ligand systems by imparting novel reactivities at the metal centers by gaining or losing electrons during catalytic processes.[11−25] Despite strong σ-donation, metal complexes
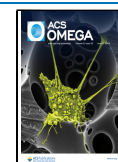
of monodentate N-heterocyclic carbene (NHC) ligands still suffer from a lack of robustness, making them less efficient as spectator or actor ligands for catalytic applications. This issue has been addressed by chelate effects inherent in bidentate and tridentate ligands bearing NHCs. While a large combination of donor atoms in pincers can be imagined, they are mostly classified based on the symmetry or the position of the anionic donor in the pincer structure. The general structures of broadly investigated bis(phenolate) NHC pincers (A-C) are shown in Figure 1. Metal complexes of these ligands, with saturated and unsaturated NHC core, have been reported with early and late transition metal ions such as Ti, Zr, Mn, Ir, Pd, and Pt.[26−33] In the majority of cases, the coplanarity of the NHC core with the tethered phenolates causes the pincer ligand to adopt a
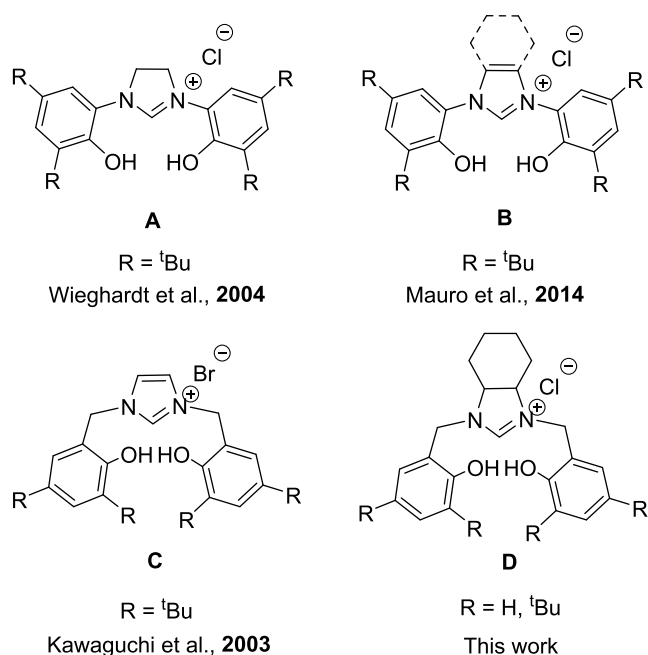
Figure 1. Previously reported tridentate OCO-donor pincer proligands (A, B, C) and a novel NHC pincer introduced in this report (D).[26−28,34]

site, herein, we introduce a novel bis aryloxide-NHC ligand that could be suitable for coordination to group VIII, such as ruthenium ions, for use as catalysts in transfer hydrogenation reactions. Transfer hydrogenation (TH) protocol, consisting in the addition of hydrogen to a substrate using a nonhydrogen gas source, is a convenient method to access various hydrogenated compounds.[35] There are many benefits of using a nonhydrogen gas source compared with more conventional methods of using pressured hydrogen gas, which is hazardous and requires elaborate experimental setups. For this reason, various transition metal complexes have been developed as catalysts in these reactions.[36−48] Most hydrogen donors employed for TH reactions, such as 2-propanol, are commercially available and inexpensive. Among transition metals, ruthenium complexes with hydrides, phosphines, and N-heterocyclic carbene ligands have been particularly investigated in TH reactions. [RuCl$_2$(PPh$_3$)$_3$], a close counterpart to Wilkinson's rhodium-based catalyst, has been one of the earliest examples of Ru(II) complexes that have been successfully used both in the traditional hydrogenation reactions with hydrogen gas and in the TH reactions.[35,49,50]

Even though most research efforts in the hydrogenation of carbonyl compounds have relied on ruthenium-, rhodium-, and iridium-based catalysts, efficient iron-based catalysts have also been developed in the past two decades. For example, different classes of iron complexes containing hydrido and carbonyls, carbonyls, diaminophosphine, and those with PNP and PNNP donor-type ligands have been developed, and excellent review articles with regard to the role of iron-based catalysts with the ligand systems mentioned above in the hydrogenation reactions have appeared recently.[35,51−54] Although scarce compared to second- or third-row transition metal ions, iron catalysts employing monodentate and bidentate N-heterocyclic carbene ligands have been reported since the beginning of this century.[54] In contrast, there are numerous literature reports about efficient bidentate or tridentate ligands bearing N-heterocyclic carbene donors with NHC-Ru(II) metal sources.[35] Owing to the important role played by the different classes of ligand systems on the efficacy of ruthenium and iron complexes in transfer hydrogenation reactions, we embarked

meridional geometry in octahedral complexes. On the contrary, pincer ligands with methylene or ethylene linkers cause distortions in five-coordinate trigonal pyramidal or square pyramidal structures, and they even adopt facial geometry in the octahedral geometry. Furthermore, less rigid pincer ligands could cause enough twisting in the ligand structure, resulting in chiral metal complexes. Therefore, the nature of aliphatic linkers of side arms could be a key factor in the structural tuning of pincer ligands.

A growing class of pincer ligands includes those that are redox-active, which are commonly known as noninnocent ligands. In search of a simple procedure for the synthesis of pincer-type chelating ligands that incorporate an NHC donor

Scheme 1. Synthesis of Pincer Proligands and Metalation Procedure: (a) NaBH$_4$, MeOH; (b) Triethylorthoformate, HCl; (c) NaBH$_4$, MeOH
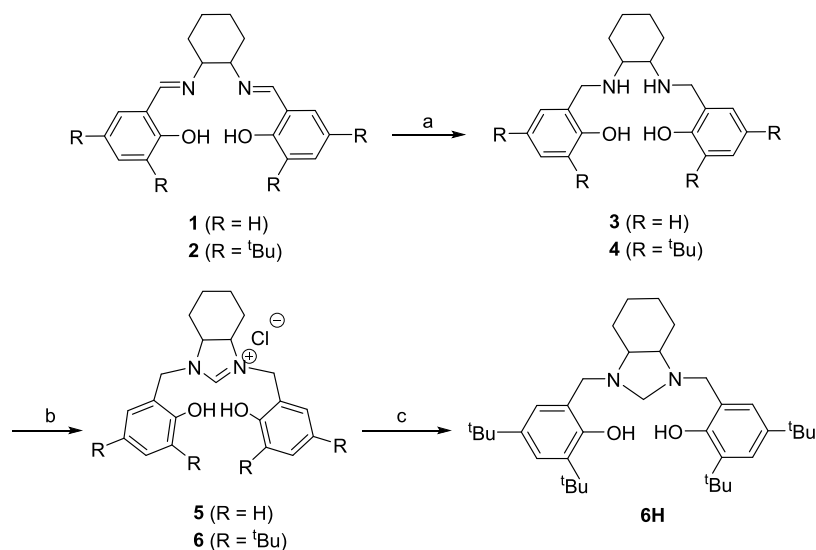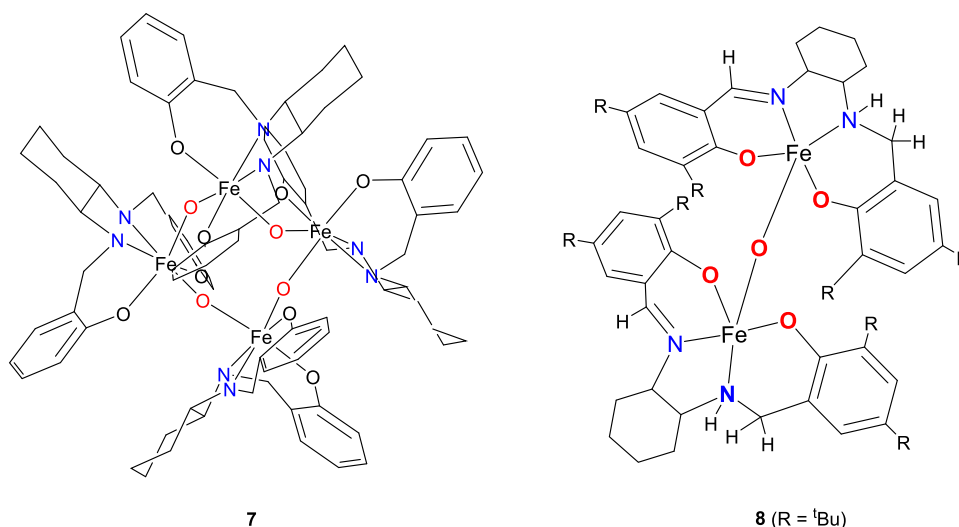
Figure 2. Sketch of **7** and **8**. For the sake of clarity, hydrogen atoms are omitted. Bridging oxygen atoms are shown in red.

on a project related to the efficient synthesis of pincer-type N-heterocyclic carbene ligands, which not only provides stability of the related metal complexes but also allows for the fine electronic and steric tuning of resulting metal complexes. We also explored the catalytic activity of these complexes in the transfer hydrogenation of ketones and aldehydes. The unexpected results from the instability and decomposition of NHC-Fe(III) complexes also provide some clues about the nature of active species in isopropyl alcohol, a common solvent for the catalytic TH reactions, which might not be species stabilized with NHC ligands and perhaps multinuclear iron-oxo or iron oxide species.

RESULTS AND DISCUSSION

Synthesis of Diphenolate Proligands and Their Fe(III) Complexes. To the best of our knowledge, there are a limited number of reports on the preparation of an NHC pincer ligand with flanking methylene bridged bis-phenols.[28,−57] In their report, Kawaguchi et al. synthesized proligand C in Figure 1 by a double alkylation reaction of the N atoms of an imidazole ring using 2-bromomethyl-4,6-di-*tert*-butylphenol. Despite the stability of the resulting titanium complex, the proligand itself is not stable under basic conditions and undergoes 1,2 alkyl migration. It is also notable that Smith et al. in 2010 reported the synthesis of a range of *N*-methyl-substituted imidazolinium salts starting with di-imine formation, with a range of aromatic aldehydes, reduction and subsequent cyclization reaction with sodium tetrafluoroborate in triethylorthoformate. The resulting C2-symmetric imidazolinium salts with flanking benzyl, naphthyl, or alkyl groups were used as precatalysts for organic transformations.[58] As an alternative procedure described in Scheme 1, we have demonstrated that the high-yielding Schiff base synthesis, its reduction, and a triethylorthoformate-promoted cyclization step could also be implemented to produce bis(phenolate) NHC pincer proligands that are flexible due to the flanking methylene bridged bis-phenols. Schiff bases **1** and **2** were synthesized according to published literature reports.[59−61] Compound **3** was achieved by slowly adding 3 equiv of sodium borohydride to a methanolic solution of **1**. In contrast, the reduction of the Schiff base **2**, due to the presence of bulky *tert*-butyl substituents, required the addition of at least 3 equiv of sodium borohydride. The ^{1}H NMR, ^{13}C

NMR, IR, and UV−vis data of **1**-**4** are provided in Supporting Information Figures S1−S11. The proligand 1,3-bis(2-hydroxybenzyl)imidazoline chloride, **5**, and 1,3-bis(4,6-di-*tert*-butyl-2-hydroxybenzyl)imidazoline chloride, **6**, were prepared in 63 and 35% yields by the cyclization reaction of **3** and **4** in acidic triethylorthoformate. The ^{1}H NMR and ^{13}C NMR data of **5** and **6** are provided in Figures S12−S19. All synthetic details of **1**-**6** are provided in the Experimental Section.

In the ^{1}H NMR spectrum of **3**, Figure S6, a series of doublets and triplets related to aromatic protons appear in the 7.20−6.82 ppm region. Diastereotopic methylene resonances, showing an AB coupling pattern, appeared as two close doublets within the 4.11−3.92 ppm region, which are often described as "roofing" where the inner two resonances approach the same frequency and gain intensity from the outer ones. The signals from cyclohexyl protons appeared as multiplets in the 2.51−1.20 ppm region. In the ^{13}C NMR spectrum of **3** in Figure S7, the appearance of six aromatic carbon signals and four aliphatic carbon signals also confirmed the clean synthesis of **3**. A similar coupling pattern for the diastereotopic methylene protons was observed in the ^{1}H NMR spectrum of **4** in Figure S10, which contains two bulky *tert*-butyl substituents on aromatic rings. The ^{1}H NMR spectra of **5** and **6** are provided in Figures S12 and S17. Singlet signals at 8.55 and 8.52 ppm belong to the NCHN proton signals in **5** and **6**, respectively, confirming the formation of a five-membered N-heterocyclic ring in precarbenes. As shown in Figures S12 and S16, the imidazoline salts **5** and **6**, owing to their less flexible core, show different coupling patterns for the diastereotopic methylene protons, which appeared between 5−4 ppm for **5** and 5−4.5 ppm for **6**. The structural rigidity of **5** and **6** is also evident in their ^{13}C NMR spectra, which show seven aromatic signals for both and eight aliphatic carbon signals for **5**. The *tert*-butyl substituents show two distinct and intense carbon signals at 30.1 and 31.5 ppm in the ^{13}C NMR spectrum of **6** in Figure S17. Based on the DEPT-135 spectrum of **5** in Figure S14, the signal at 161.7 ppm could be unambiguously assigned to the central = CH from the heterocyclic ring. Likewise, the heterocyclic = CH signal in **6** appeared at 160.6 ppm, as shown in Figure S17. Attempts to obtain solid-state structures of 5 or 6 were also unsuccessful and only reduction of 6 to 6H allowed the obtainment of its

single-crystal structure data, thus confirming hydroxyl donor sites in these ligands that could span trans positions. In the solid-state structure of 6H in Figure S29, two substituted aromatic rings are twisted in opposite directions as a result of the presence of flexible methylene bridges and bulky tert-butyl substitutes, which allows hydroxyl substitutes to be arranged in the opposite ends so that upon coordination, along with the central carbene center, three coplanar sites around the metal center could be occupied. This type of meridional configuration in the pincer-type ligands was previously observed in group IV chemistry and allowed for the formation of stable metal complexes.[9]

The metalation of 5 and 6 was attempted using both Fe(II) and Fe(III) salts. 7 and 8 were synthesized in dry THF solvent by reacting 1 equiv of the imidazoline salt 5 with 3 equiv of potassium tert-butoxide, followed by the addition 1 equiv of FeCl$_3$. Then, the mixture was refluxed at 70 °C for 12 h. The potassium chloride byproduct was removed by centrifugation, and the supernatant was concentrated under reduced pressure. The residue was dissolved in dichloromethane, washed with deionized water, and then dried under a vacuum, giving 7 as a fine dark red powder. Suitable for X-ray experiments, red block crystals of complex 7 were obtained from a methanol/diethyl ether solution at room temperature. As shown in Figure 2, complex 7 is an Fe(III) complex where the carbon center from carbene ligand was lost, and each Fe(III) center adopted an octahedral configuration by the coordination of two nitrogen from cyclohexyl amine, two phenolate oxygens, and μ_2-oxo-bridged atoms. Complex 7 crystallized in the tetragonal space group $P4_2/n$. The asymmetric unit contains a quarter of the tetranuclear unit, as shown in Figure 3. The selected bond distances and angles are given in the caption to Figure 3. Similar to literature reports of oxo-bridged iron(III) complexes, the Fe−O−Fe unit in 7 is nonlinear (131.71°). A rare case of iron(III) complex with Fe−O−Fe angle of 180.0° has
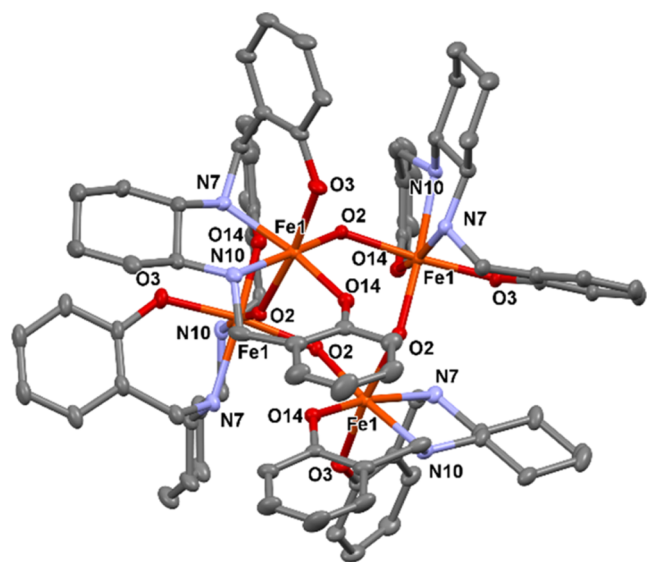

Figure 3. Ellipsoid plot of Fe(III) tetramer, 7. Hydrogen atoms have been omitted for clarity. Selected bond lengths (Å), bond angles [°]: Fe1−O3, 1.974(4); Fe1−O2^i, 2.041(4); Fe1−O14, 1.933(4); Fe1−N10, 2.201(5); Fe1−N7 2.145(6); O3−Fe1−O2^i, 172.5(2); O2−Fe1−O14, 96.39(17); N7−Fe1−N10, 79.3(2); N7−Fe1−O14, 166.9(2); N10−Fe1−O2, 174.2(2). Symmetry code: (i) y, 1.5-x, 1.5-z.

also been reported.[62] The IR spectrum of 7 in Figure S23 shows intense signals for N−H vibrations in the region around 3300 cm^{-1}. The molecular structures of the major products of metalation of 5 or 6 with FeCl$_3$ are shown in Figure S28. It is notable that metalation of 5 or 6 with FeCl$_3$ in dry acetonitrile gave similar products. The metalation of bulkier ligand 6 using FeCl$_3$, on the other hand, gave light pink crystals and a dark red powder upon crystallization in methanol layered with a few drops of ether. The light pink crystals turned out to be an altered form of the NHC ligand where N-alkylation of amine nitrogen has occurred, 7H. At this point, two vastly different outcomes for the reactivity of 5 and 6 with FeCl$_3$ are not easily understood. In both cases, carbene's central carbon atom has been lost, and in the case of 7, the resulting bis-aminophenol structure, which is similar to 3, had participated in the formation of a tetrameric iron complex. In the case of 6, however, the bulky ligand has taken a different reaction pathway, where amino group alkylation occurred. This is not too surprising, given that there are plenty of literature reports on using methanol or ethanol for the alkylation of primary and secondary amines.[63] There are also literature reports on ligand structural changes upon reaction with metal chlorides. For example, palladium chloride, when used instead of palladium acetate, instead of coordination could modify ortho-amino-phenolates into benzooxazol-type compounds.[34] Each asymmetrical unit in the solid-state structure of 7H is composed of two different organic molecules, and the presence of N−CH$_2$OH units in each molecule is possibly the result of a nucleophilic attack on the five-membered NHC ring by the methanol. The metalation of 6 with iron(II) bromide was also investigated using a similar procedure described above for the iron(III) chloride complex, which led to the formation of an iron(III) binuclear complex with only one μ-oxo-bridged ligand. While the loss of a carbon atom in 5, in forming complex 7 during the metalation process, has led to the formation of two amine functional groups (R$_2$NH), the loss of a carbon atom from the N-heterocyclic ring in 6 has led to the formation of two different functional groups amine (R$_2$NH) and imine (RN = CH) in complex 8. As shown in Figure 2, complex 8 is a binuclear Fe(III) complex where the carbon center from N-heterocyclic ring in 6 was lost, and each Fe(III) center adopted a distorted square bipyramidal geometry by the coordination from two nitrogen from neutral cyclohexyl amine and imine, and μ-oxo-bridged atom. The crystallization process of 8 was successful only in three solvent media, including dichloromethane and acetonitrile layered with a few drops of diethyl ether. The single-crystal structure of 8 is shown in Figure 4. Similar to complex 7, the IR spectrum of 8 in Figure S25 shows intense signals for N−H vibrations in the region around 3300 cm^{-1}. Oxo ligands are capable of stabilizing high oxidation state metal ions.[64] Metal-oxo complexes are highly important intermediates in oxidation reactions catalyzed by using metal complexes. They could also be used as oxygen-atom transfer agents in many organic reactions.[65] Oxo complexes of molybdenum and iron have shown many important biological important oxidation reactions.[66−71]

Electrochemical Behavior of the Ligands and the Related Complexes. Figure 5 shows the cyclic voltammogram of compound 6 in 0.1 M tetrabutylammonium tetrafluoroborate as a supporting electrolyte in acetonitrile in the range of −2.5 to +1.5 V vs Fc+/Fc at 100 mV/s. The arrows in the figure show the potential scan route. The potential scan started from −0.4 V toward the negative
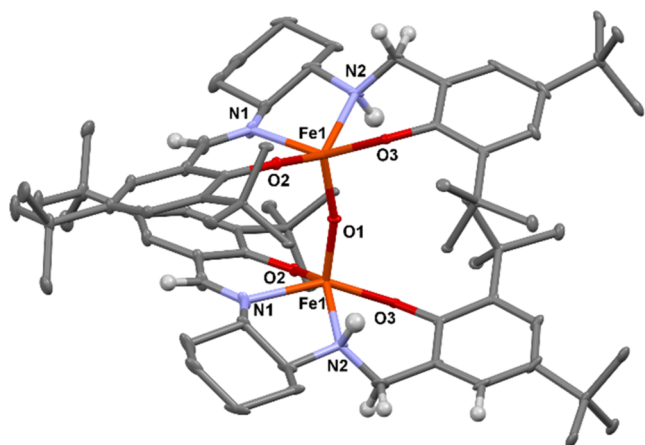
Figure 4. Ellipsoid plot of compound **8**. Hydrogen atoms are omitted for clarity. Selected bond lengths [Å], bond angles [°]: Fe1−O1, 1.7744(4); Fe1−O2, 1.9038(17); Fe1−O3, 1.9073(15); O1−Fe1−O2, 111.69(6); O1−Fe1−O3, 109.05(8); O2−Fe1−O3, 92.02(7); Fe1−O1−Fe1 164.39(15); Fe1−O2−C9, 132.00(15); Fe1−O3−C16, 128.92(14).
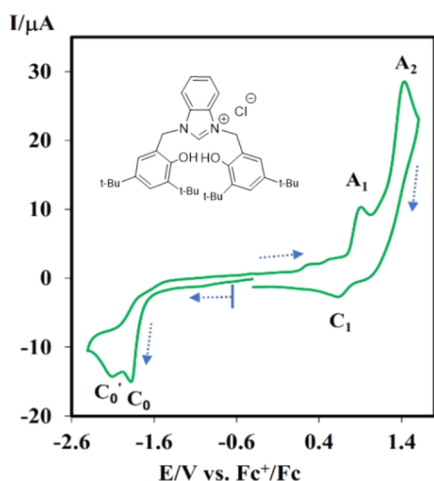

Figure 5. Cyclic voltammogram of 10 mM **6** at a glassy carbon electrode in 0.1 M [Bu$_4$N][PF$_6$] in acetonitrile at a scan rate of 100 mV/s.

direction up to −2.5 V, and in the reverse scan, the potential was scanned from −2.5 to +1.5 V. In the second cycle, it continued to −0.4 V. Upon exerting potential toward negative values, two irreversible cathodic peaks (C0′, C0) were observed at the potentials −1.98 and −2.12 V. According to
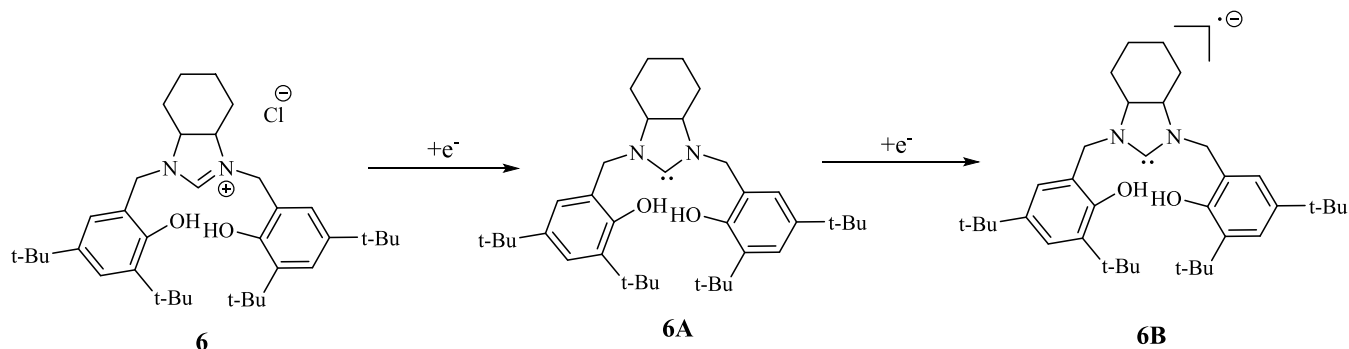
literature surveys, the signals are attributed to electrochemical reduction of **6** to anion radical during two successive one-electron transfer processes (Scheme 2).[72,73]

By scanning toward positive potentials, two anodic signals were observed at +0.86 and +1.4 V (A1, A2). In addition, the cathodic counterpart of the anodic peak of A1 (C1) appeared at +0.5 V in the second cycle. Previously published papers reported the oxidation of similar compounds during a single two-electron transfer process (eq 1).[74] However, the oxidation of **6** proceeds via two consecutive one-electron oxidations (eqs 2 and 3), probably due to its asymmetrical structure and the presence of one positive charge in the compound.

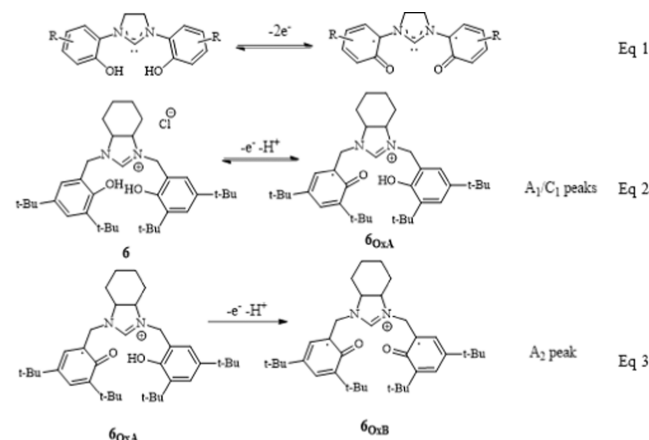Equations 1−3 show the proposed mechanism of oxidation of **6**.

Figure 6 shows cyclic voltammograms (I) and normalized voltammograms (II) (normalization was performed by dividing the current by the square root of the scan rate) of compound **6** in the range of −0.4 to +1.1 V at different scan rates. The anodic signal indicated an irreversible feature at a low scan rate of 50 mV s^{-1}. The cathodic peak (C1) appeared by increasing the potential scan rate, and its intensity increased. This observation reveals the instability of the oxidation product arising from the presence of a positive charge in the structure.

Catalytic Activity of Metal Complexes in Catalytic Transfer Hydrogenation. Initially, the catalytic hydrogenation of acetophenone was conducted under metal-free conditions using only **5** and **6** as the catalyst. 1-Phenylethanol was obtained in 40% yield using these proligands. Transfer hydrogenation of carbonyl compounds is sensitive to temperature, the nature of the base, and the type of solvent. Therefore, conversion to 1-phenylethanol was conducted using
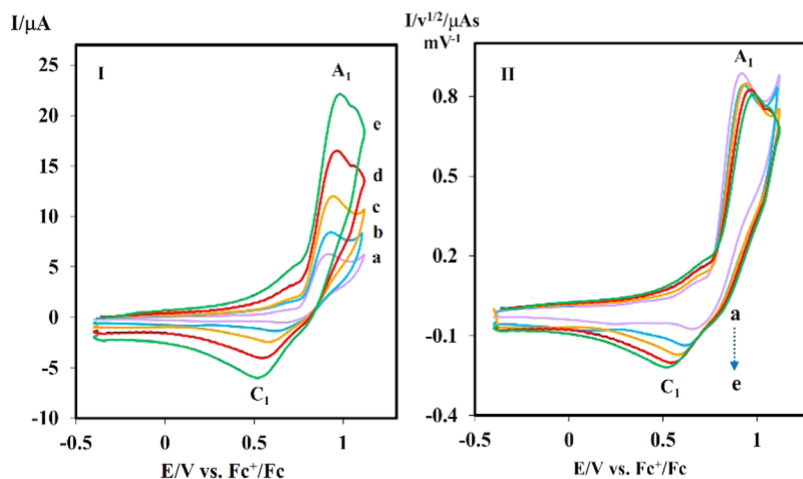
Scheme 2. Consecutive 1 Electron Oxidation of 6

Figure 6. Cyclic voltammograms (I) and normalized cyclic voltammograms (II) of 10 mM **6** in 0.1 M $[Bu_4N][PF_6]$ in acetonitrile at different scan rates of (a−e) 50, 100, 200, 400, and 750 mV/s.

7 and **8** in 2-propanol, methanol, and ethanol as hydrogen sources. 2-Propanol turned out to be a more suitable solvent. The catalytic reactions were also performed at room temperature, at 50 °C, and at the refluxing temperature of 2-propanol. The optimal conversion was achieved at 82 °C. Sodium and potassium salts such as potassium hydroxide, potassium tert-butoxide, potassium carbonate, and sodium hydroxide are the commonly utilized bases in the transfer hydrogenation reactions. During reaction optimizations, higher conversions were obtained with potassium hydroxide and potassium tert-butoxide using both Fe(III)-based catalysts. Therefore, the rest of the TH reactions were conducted using less air-sensitive and cheaper potassium hydroxide. Notably, the amount of KOH, when adjusted to 4 mmol, gave the optimum result. The presence of *tert*-butyl substitutes in the ligand did not seem to influence reaction outcome highly; therefore, further reaction optimizations were conducted using **7**. The optimized reaction condition for TH of acetophenone catalyzed is summarized in Table S2. In the reaction runs and under an N_2 atmosphere, acetophenone (1.0 mmol) was added to a solution containing iron catalyst **7** (∼4 mg/0.002 mmol) and 2-propanol (5.0 mL), and the mixture was stirred under reflux at 82 °C for 30 min. Then, KOH (4 mmol) was added, and the mixture color immediately changed to dark brown. The reaction continued for 24 h, and reaction yield was determined by gas chromatography. Under optimized reaction conditions, a variety of aryl and alkyl aldehydes were examined for the scope of this reaction. As shown in Table 1, in most cases, **7** catalyzed the formation of the desired products in excellent yields.

While the nature of active species in this catalytic reaction is highly dependent on the type of metal and ligands utilized, two mechanisms involving inner sphere and outer sphere hydride transfer to the substrate are proposed as major steps in the homogeneous TH reaction catalyzed by Fe(III) complexes.[75] In addition, another mechanism involving alkoxide species has been proposed.[75] Due to the sensitivity of the complexes introduced in this research to solvent media, at this point, it is not clear whether these catalysts follow the general mechanisms introduced before. Therefore, the exploration of mechanisms by which **7** catalyze TH of carbonyl compounds summarized in Table 1 is the subject of future studies.
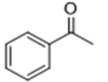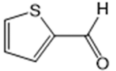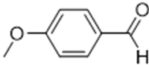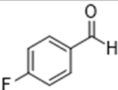
CONCLUSIONS
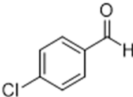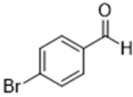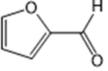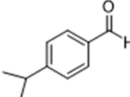
The synthesis and characterization of novel pincer-type proligands with a central N-heterocyclic carbene donor is introduced. The chloride salts of the proligands were obtained in high yields and had benchtop stability for several months. The electrochemical behavior of novel proligands shows that these proligands undergo two consecutive one-electron oxidation processes, in contrast to the single two-electron oxidation process observed in similar compounds. The complexation of these proligands was carried out, and the initially intended metal complexes turned out to be highly air- and moisture-sensitive, leading to the formation of iron(III)-oxo complexes, supported with amine and imine functional groups, lacking any carbene functional group. The Fe(III) complexes of these novel proligands were tested in the transfer hydrogenation of selected carbonyl compounds. The results from catalytic reactions reveal that these complexes can catalyze TH reactions in minimal quantity and with high efficiency.

EXPERIMENTAL SECTION

Reagents and solvents were used as received from commercial suppliers. All syntheses were carried out under a nitrogen atmosphere using a dry flame-dried flask. Solvents were dried u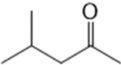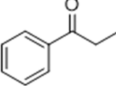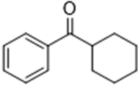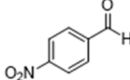sing standard methods. Infrared spectra were recorded on a Bruker Vector 22 FTIR spectrometer (ATR in the range 400−4000 cm^{-1}). NMR spectra in solution were recorded on a Bruker AV-400 spectrometer with $SiMe_4$ for ^1H and ^{13}C as external references. Cyclic voltammetry experiments were carried out using Autolab PGSTAT 101 monitored by software of NOVA with a typical three-electrode cell configuration equipped with a glassy carbon disk (1.8 mm diameter), Pt rod, and Ag wire as working, counter, and pseudoreference electrodes, respectively. The potentials were reported versus the ferrocene/ferrocenium (Fc+/Fc) redox couple.

Synthesis of 1. To a solution of 1,2-diaminocyclohexane (2.0 g, 17.6 mmol) in methanol was added 2-hydroxybenzaldehyde (4.3 g, 35.2 mmol). Then, 4 drops of formic acid catalyst were added, and the mixture was stirred at ambient temperature for 3 h. The light-yellow precipitate was filtered off and dried under a vacuum. Yield: 3.0 g, 53%. The corresponding spectra are provided in Figures S1−S3. ^1H

Table 1. Catalytic Transfer Hydrogenation of Aldehydes and Ketones Using 7[a]

#	Substrate	Yield (%)
1		96
2		99
3		97
4		99
5		> 99
6		97
7		99
8		99
9		37
10		86
11		58
12		99

[a]Reactions were conducted in a flask (25 mL) with 1 mmol ketone, 5 mL of isopropyl alcohol, 4 mmol of KOH, and 0.002 mmol of 7 at 82 °C. TON (with catalyst 7) = 1444, Time 24 h.

NMR (Acetone-d_6, 400 MHz): δ 13.12 (s, 2H), 8.49 (s, 2H), 7.31 (d, 2H, ^3J = 8.0 Hz), 7.27 (t, 2H, ^3J = 8.0 Hz), 6.83 (d, 2H, ^3J = 8.0 Hz), 6.81 (t, 2H, ^3J = 8.0 Hz), 2.09−1.54 (m, 10H). ^{13}C{^{1}H} NMR (Acetone-d_6, 100 MHz) δ: 165.3, 161.0, 132.0, 131.6, 118.9, 116.4, 72.5, 32.9, 24.0. FTIR (KBr, cm^{-1}):

3004 (w), 2924 (m), 2846 (m), 1623(s), 1496(s), 1413(s). UV−vis. In CH$_2$Cl$_2$, λ_{max}/nm: 217, 255, 317.

Synthesis of 2. To a solution of 1,2-diaminocyclohexane (1.316 g, 11.54 mmol) in methanol was added 3,5-di-tert-butyl 2-hydroxybenzaldehyde (5.411 g, 23 mmol). Then, 4 drops of acetic acid catalyst were added and the mixture was stirred at ambient temperature for 3 h. A light-yellow precipitate was filtered off, washed with ether, and dried under vacuum. Yield: 2.0 g, 31%. The corresponding spectra are provided in Figures S4 and S5. ^{1}H NMR (CDCl$_3$, 250 MHz): δ 13.52 (s, 2H), 8.31 (s, 2H), 7.31 (s, 2H), 6.99 (s, 2H), 3.45−3.28 (m, 2H), 2.05−1.66 (s, 8H), 1.41 (s, 18 H), 1.24 (s, 18H). ^{13}C NMR (CDCl$_3$, 100 MHz) δ: 165.8, 157.9, 139.8, 136.3, 126.7, 126.0, 117.8, 72.4, 34.9, 33.2, 31.4, 29.4, 24.3.

Synthesis of 3. Over a period of 1 h, sodium borohydride (1.05 g, 27.9 mmol) was added in small portions to a solution of **1** (3.0 g, 9.3 mmol) in 10 mL of methanol at room temperature. The slurry was stirred for 24 h, then 30 mL of deionized water was added, and after stirring for 10 min, the organic phase was extracted with dichloromethane (3 × 15 mL). The volatile solvent was removed under reduced pressure, yielding a white powder. Yield: 1.2 g, 59%. The corresponding spectra are provided in Figures S6−S9. ^{1}H NMR (CDCl$_3$, 400 MHz): δ 7.20 (t, 2H, ^3J = 4.0 Hz), 7.02 (d, 2H, ^3J = 8.0 Hz), 6.87−6.82 (m, 4H), 4.09 (d, 2H, ^2J = 12.0 Hz), 3.98 (d, 2H, 2J = 12.0 Hz), 2.51−2.46 (m, 2H), 2.21−2.17 (m, 2H), 1.76−1.68 (m, 2H), 1.31−1.20 (m, 4H). ^{13}C{^{1}H} NMR (CDCl$_3$, 100 MHz) δ: 158.0, 128.9, 128.3, 122.9, 118.4, 114.8, 57.6, 44.8, 28.2, 24.2. FTIR (KBr, cm^{-1}): 3322 (m), 3297 (m), 3052 (w), 2925 (m), 2850 (w), 1590 (m), 1452 (s), 1261 (m). UV−vis. In CH$_3$CN, λ_{max}/nm: 225, 275.

Synthesis of 4. The successful reduction of **2** (2.0 g, 3.65 mmol) could be accomplished quickly by the instantaneous addition of three equiv of sodium borohydride. Or, it could be done over a period of 1 h by the addition of 15 equiv of sodium borohydride in small portions (4.150 g, 109.7 mmol) in 60 mL of methanol at room temperature, resulting in a fine powder. Then, 40 mL of deionized water was added, and after stirring for 10 min, a white-colored precipitate was collected by filtration. Yield: 1.50 g, 74%. The corresponding spectra are provided in Figures S10 and S11. ^{1}H NMR (CDCl$_3$, 250 MHz): δ 10.72 (s, 2H), 7.25 (s, 2H), 6.89 (s, 2H), 4.20−3.78 (m, 4H), 2.69−2.37 (m, 2H), 2.37−2.06 (m, 2H), 1.78−1.65 (m, 4H), 1.39 (s, 18H), 1.30 (s, 18H). ^{13}C NMR (CDCl$_3$, 100 MHz) δ: 154.4, 140.6, 135.9, 123.1, 123.0, 122.4, 59.9, 50.8, 34.8, 34.2, 31.7, 29.6, 24.1.

Synthesis of 5. Compound **3** (1.2 g, 3.06 mmol) was dissolved in 5.0 mL of triethylorthoformate and was heated under reflux at 70 °C until all diamine was completely dissolved. (Note: Fully dissolving starting diamine material is a crucial step, and it might take as much as 0.5 h or longer to do so). Then, to the obtained clear solution was added concentrated HCl (1N, 0.39 mL, 1.3 mmol) in about 5 min, and the reaction mixture was stirred for 1 h. After the cooling reaction mixture, the solvent was evaporated, and the resulting viscous product was triturated with Et$_2$O. The fine white powder was filtered and dried under nitrogen. Yield: 0.87 g, 63%. The related spectra are provided in Figures S12−S16. ^{1}H NMR (CDCl$_3$, 400 MHz): δ 9.96 (s, 2H), 8.55 (s, 1H), 7.33 (d, 2H, ^3J = 8.0 Hz), 7.19 (t, 2H, ^3J = 8.0 Hz), 7.01 (d, 2H, ^3J = 8.0 Hz), 6.75 (t, 2H, ^3J = 8.0 Hz), 4.51 (d, 2H, ^2J = 12.0 Hz), 4.61 (d, 2H, ^2J = 12.0 Hz), 3.23−3.12 (m, 2H), 2.21−

2.18 (m, 2H), 1.39−1.27 (m, 2H), 1.20−1.10 (m, 2H). $^{13}C\{^1H\}$ NMR (CDCl$_3$, 100 MHz) δ: 161.7, 156.6, 130.9, 130.3, 119.3, 118.4, 116.9, 66.9, 57.2, 47.8, 46.8, 27.3, 23.6, 22.4, 18.0. $^{13}C\{^1H\}$ NMR (CDCl$_3$, 100 MHz) δ: 160.6, 152.2, 143.0, 140.1, 125.4, 125.0, 121.3, 67.4, 59.4, 48.7, 35.0, 34.2, 31.5, 30.1, 27.5, 23.7, 14.9. FTIR (KBr, cm^{-1}): 3065 (9s), 2949 (s), 2861 (m), 1644 (m), 1606 (s), 1503 (m), 1457 (s), 1354 (m), 1273 (m). UV−vis. In CH3CN, λ_{max}/nm: 219, 240, 274.

Synthesis of 6. Compound **4** (1.0 g, 1.814 mmol) was dissolved in 10.0 mL of triethylorthoformate and was heated under reflux at 70 °C until all diamine was completely dissolved. (Note: Fully dissolving starting diamine material is a crucial step, and it might take as much as 30 to 60 min to do so). Then, to the obtained clear solution was added concentrated HCl (1N, 0.191 mL, 1.3 mmol) in 5 min, and the reaction mixture was stirred at 70 °C for 3 h. Depending on the quantity of the starting materials, the reaction described above might last up to 24 h to complete.

After the reaction mixture was cooled, the precipitates were collected by filtration and triturated with Et$_2$O. Fine white powder was collected by filtration. Yield: 0.384 g, 35%. The related spectra are provided in Figures S17−S20. ^1H NMR (CDCl$_3$, 250 MHz): δ 8.52 (s, 1H), 7.82 (s, 2H), 7.27 (s, 2H), 6.88 (s, 2H), 4.98 (d, 2H, ^3J = 12.5 Hz), 4.55 (d, 2H, ^3J = 12.5 Hz), 3.38−3.34 (m, 2H), 2.19−2.14 (m, 2H), 1.84−1.82 (m, 2H), 1.52−1.45 (m, 4H), 1.38 (s, 18H), 1.22 (s, 20H). $^{13}C\{^1H\}$ NMR (CDCl$_3$, 63 MHz) δ: 160.6, 152.2, 143.0, 140.1, 125.4, 125.0, 121.3, 67.4, 59.4, 48.2, 35.0, 34.2, 31.5, 30.1, 27.5, 23.7, 14.9. FTIR (KBr, cm^{-1}): 3005 (m), 2958 (s), 2911 (w), 2866 (m), 1610 (s), 1480 (s), 1448 (m). UV−vis. in CH$_3$CN, λ_{max}/nm: 206, 223, 247, 278.

Synthesis of 6H. To compound **6** (0.03 g, 0.048 mmol) in methanol was added NaBH$_4$ (0.004 g, 0.095 mmol) over 10 min. Then, the mixture was stirred for 45 min. After adding 2 mL of deionized water, the mixture was stirred for 0.5 h. The white-colored precipitate was filtered and dried in an oven. Yield: 0.015 g, 53%. The related spectra are provided in Figures S21 and S22. ^1H NMR (CDCl$_3$, 250 MHz): δ 10.68 (s, 2H), 7.19 (s, 2H), 6.79 (s, 2H), 4.15 (d, 2H, ^2J = 15.0 Hz), 3.54 (s, 2H), 3.48 (d, 2H, ^2J = 15.0 Hz), 2.36−2.33 (m, 2H), 2.04−2.0 (m, 2H), 1.84−1.74 (m, 2H), 1.41−1.26 (m, 42H). $^{13}C\{^1H\}$ NMR (CDCl$_3$, 63 MHz) δ: 153.9, 140.7, 135.6, 123.0, 120.9, 77.5, 77.0, 76.5, 75.5, 69.5, 57.3, 34.8, 34.1, 31.6, 29.5, 29.0, 24.1.

Synthesis of 7. Compound **5** (0.130 g, 0.35 mmol) was dissolved in dry THF. KO^{t}Bu (0.117 g, 1.04 mmol) and FeCl$_3$.6H$_2$O (0.094 g, 0.35 mmol) were added, respectively. The mixture was refluxed at 70 °C for 24 h. The precipitate was collected by centrifugation and was discarded. The supernatant was concentrated under reduced pressure, which gave a dark red solid. The red solid was dissolved in dichloromethane, washed with deionized water, and dried under vacuum. Yield: 0.085 g, 62%. The related spectra are provided in Figures S23 and S24. FTIR (KBr, cm^{-1}): 3056 (m), 2948 (s), 2853 (m), 1642 (s), 1598 (s), 1445 (m). UV−vis. in CH$_3$CN, λ_{max}/nm: 206, 278, 460. Anal. Calcd for C$_{80}$H$_{96}$Fe$_4$N$_8$O$_{12}$: C, 60.62; H, 6.10; N, 7.07. Found: C, 60.50; H, 6.01; N,7.00.

Synthesis of 8 Using FeCl$_3$. Compound **6** (0.1 g, 0.168 mmol) was dissolved in dry THF. KO^{t}Bu (0.056 g, 0.50 mmol), then FeCl$_3$.6H$_2$O (0.045 g, 0.168 mmol) were added,

respectively. The mixture was refluxed at 70 °C for 24 h. The precipitate was collected by centrifugation and discarded. The supernatant was concentrated under reduced pressure, which gave a dark red solid. The red solid was dissolved in dichloromethane, washed with deionized water, and dried under vacuum. Yield: 0.060 g, 56%. The related spectra are provided in Figures S25 − S27. FTIR (KBr, cm^{-1}): 2951 (s), 2863 (m), 1644 (s), 1602 (m), 1464 (m). UV−vis. in CH$_3$CN, λ_{max}/nm: 208, 225, 282. ^{13}C NMR (63 MHz, CDCl$_3$) δ: 164.8, 154.1, 153.6, 152.4, 152, 140.9, 137.7, 136, 125.8, 124.9, 123, 121.3, 64.6, 58.3, 50.1, 35.2, 34.8, 33.9, 31.7, 29.6, 25.4, 24.5. Anal. Calcd for C$_{72}$H$_{108}$Fe$_2$N$_4$O$_5$: C, 70.81; H, 8.91; N, 4.59. Found: C, 70.75; H, 8.88; N,4.60.

Synthesis of 8 Using FeBr$_2$. Compound **6** (0.1 g, 0.168 mmol) was dissolved in dry THF. KO^{t}Bu (0.093 g, 0.83 mmol), then FeBr$_2$ (0.045 g, 0.168 mmol) were added, respectively. The mixture was refluxed at 70 °C for 24 h. The precipitate was collected by centrifugation and discarded. The supernatant was concentrated under reduced pressure, which gave a dark red solid. The red solid was dissolved in dichloromethane, washed with deionized water and dried under vacuum. Yield: 0.07 g, 58%.

General Condition for Transfer Hydrogenation Reaction Optimization. A solution of acetophenone (0.060 g, 0.5 mmol), complex **7** (0.002 mmol), and KOH (4 mmol) in isopropyl alcohol (5 mL) was refluxed for 24 h at about 82 °C in an oil bath. The reaction mixture was then cooled down to room temperature and passed through a short silica column to remove the metal complex. The crude product was analyzed by GC.

X-ray Crystal Structure Determination and Refinement. Crystals of **6H** were grown in acetonitrile layers with a few drops of ether. Crystals of **7** and **7H** were grown in methanol/ether and methanol, respectively. Crystals of **8** were grown in a dichloromethane/acetonitrile mixture layered with diethyl ether. The X-ray diffraction data of samples were collected with Rigaku OD Supernova using Atlas S2 CCD detector and mirror collimated Cu−Kα (λ = 1.54184 Å) from a microfocused sealed X-ray tube. The samples were cooled to 95 K during the measurement. Integration of the CCD images, absorption correction, and scaling were done by program CrysAlisPro 1.171.41.123a (Rigaku Oxford Diffraction, 2022). Crystal structures were solved by charge flipping with program SUPERFLIP.[76] Structures **6H** and **7H** were refined with the Jana2020[77] program package, while structure **7** was refined with Crystals.[78] In both cases, the structures were refined by the full-matrix least-squares technique on F2. The molecular structure plots were prepared by Mercury 2020.1.[79] All fully occupied hydrogen atoms were visible in difference Fourier maps and were kept in the geometrically correct positions with a C−H distance of 0.96 Å. The hydrogen atoms attached to oxygen and nitrogen atoms were refined with a restrained geometry. In the case of structure **7**, the hydrogen atoms attached to nitrogen were placed in ideal positions and refined with riding constraints. The isotropic atomic displacement parameters of hydrogen atoms were evaluated as 1.2 equiv of the parent atom. Structure **7H** has two disordered systems in it. The disordered *tert*-butyl group was refined with restrained geometry, and the sum of occupancies was constrained to 1, resulting in a final occupancy ratio of 0.723(3):0.277(3). The disorder of methyl C31a and hydrogen was refined freely, with the sum of occupancies constrained to 1 resulting in occupancy ratio 0.676(8):0.324(8) methyl:hydrogen. Crystallographic

data, details of the data collection, structure solution, and refinements are listed in Table S1.

ASSOCIATED CONTENT

Supporting Information
The Supporting Information is available free of charge at https://pubs.acs.org/doi/10.1021/acsomega.4c02602.

Crystallographic data 1 (CIF)
Crystallographic data 2 (CIF)
Crystallographic data 3 (PDF)
Crystallographic data 4 (CIF)
Crystallographic data 5 (CIF)
Spectroscopic data and NMR line shape analysis (Figures S1–S26) (Tables S1 and S2) (PDF)

Accession Codes
CCDC numbers 2285374, 2285376, 2285375, and 2338568 contain the supplementary crystallographic data for **6H, 7, 7H,** and **8**, respectively. These data can be obtained free of charge via http://www.ccdc.cam.ac.uk/conts/retrieving.html, or from the Cambridge Crystallographic Data Centre, 12 Union Road, Cambridge CB2 1EZ, UK; fax: (+44) 1223−336−033; or e-mail: deposit@ccdc.cam.ac.uk.

AUTHOR INFORMATION

Corresponding Author
Abdollah Neshat − *Department of Chemistry, Institute for Advanced Studies in Basic Sciences (IASBS), Zanjan 45137-66731, Iran;* orcid.org/0000-0002-1424-2292; Email: a.neshat@iasbs.ac.ir

Authors
Ali Mousavizadeh Mobarakeh − *Department of Chemistry, Institute for Advanced Studies in Basic Sciences (IASBS), Zanjan 45137-66731, Iran*

Mohammad Reza Yousefshahi − *Department of Chemistry, Institute for Advanced Studies in Basic Sciences (IASBS), Zanjan 45137-66731, Iran*

Fahimeh Varmaghani − *Department of Chemistry, Institute for Advanced Studies in Basic Sciences (IASBS), Zanjan 45137-66731, Iran*

Michal Dusek − *Institute of Physics of the Czech Academy of Sciences, 18221 Prague 8, The Czech Republic;* orcid.org/0000-0001-9797-2559

Vaclav Eigner − *Institute of Physics of the Czech Academy of Sciences, 18221 Prague 8, The Czech Republic;* orcid.org/0000-0003-1014-3980

Monika Kucerakova − *Institute of Physics of the Czech Academy of Sciences, 18221 Prague 8, The Czech Republic*

Complete contact information is available at:
https://pubs.acs.org/10.1021/acsomega.4c02602

Notes
The authors declare no competing financial interest.

ACKNOWLEDGMENTS

REFERENCES
(1) Moulton, C. J.; Shaw, B. L. Transition Metal−Carbon Bonds. Part XLII. Complexes of Nickel, Palladium, Platinum, Rhodium and Iridium with the Tridentate Ligand 2,6-Bis[(Di-t-Butylphosphino)-Methyl]Phenyl. *J. Chem. Soc., Dalton Trans.* **1976**, No. 11, 1020−1024. No.
(2) Taakili, R.; Canac, Y. NHC Core Pincer Ligands Exhibiting Two Anionic Coordinating Extremities. *Molecules* **2020**, 25, 2231.
(3) van der Vlugt, J. I. *Redox-Active Pincer Ligands BT - Metal-Ligand Co-Operativity: Catalysis and the Pincer-Metal Platform*; van Koten, G.; Kirchner, K.; Moret, M.-E., Eds.; Springer International Publishing: Cham, 2021; pp 135−179 DOI: 10.1007/3418_2020_68.
(4) Vogt, M.; Langer, R. The Pincer Platform Beyond Classical Coordination Patterns. *Eur. J. Inorg. Chem.* **2020**, 2020 (41), 3885−3898.
(5) Alig, L.; Fritz, M.; Schneider, S. First-Row Transition Metal (De)Hydrogenation Catalysis Based On Functional Pincer Ligands. *Chem. Rev.* **2019**, 119 (4), 2681−2751.
(6) Peris, E.; Crabtree, R. H. Key Factors in Pincer Ligand Design. *Chem. Soc. Rev.* **2018**, 47 (6), 1959−1968.
(7) van Koten, G. Tuning the Reactivity of Metals Held in a Rigid Ligand Environment. *Pure Appl. Chem.* **1989**, 61 (10), 1681−1694, DOI: 10.1351/pac198961101681.
(8) Lawrence, M. A. W.; Green, K.-A.; Nelson, P. N.; Lorraine, S. C. Pincer Ligands—Tunable, Versatile and Applicable. *Polyhedron* **2018**, 143, 11−27.
(9) Pugh, D.; Danopoulos, A. A. Metal Complexes with 'Pincer'-Type Ligands Incorporating N-Heterocyclic Carbene Functionalities. *Coord. Chem. Rev.* **2007**, 251 (5−6), 610−641.
(10) Curley, J. B.; Townsend, T. M.; Bernskoetter, W. H.; Hazari, N.; Mercado, B. Q. Iron, Cobalt, and Nickel Complexes Supported by a IPrPNPhP Pincer Ligand. *Organometallics* **2022**, 41 (3), 301−312.
(11) Luca, O. R.; Crabtree, R. H. Redox-Active Ligands in Catalysis. *Chem. Soc. Rev.* **2013**, 42 (4), 1440−1459.
(12) Adhikari, D.; Mossin, S.; Basuli, F.; Huffman, J. C.; Szilagyi, R. K.; Meyer, K.; Mindiola, D. J. Structural, Spectroscopic, and Theoretical Elucidation of a Redox-Active Pincer-Type Ancillary Applied in Catalysis. *J. Am. Chem. Soc.* **2008**, 130 (11), 3676−3682.
(13) Szigethy, G.; Heyduk, A. F. Aluminum Complexes of the Redox-Active [ONO] Pincer Ligand. *Dalton Trans.* **2012**, 41 (26), 8144−8152.
(14) Harris, C. F.; Bayless, M. B.; van Leest, N. P.; Bruch, Q. J.; Livesay, B. N.; Bacsa, J.; Hardcastle, K. I.; Shores, M. P.; de Bruin, B.; Soper, J. D. Redox-Active Bis (Phenolate) N-Heterocyclic Carbene [OCO] Pincer Ligands Support Cobalt Electron Transfer Series Spanning Four Oxidation States. *Inorg. Chem.* **2017**, 56 (20), 12421−12435.
(15) O'Reilly, M. E.; Veige, A. S. Trianionic Pincer and Pincer-Type Metal Complexes and Catalysts. *Chem. Soc. Rev.* **2014**, 43 (17), 6325−6369.
(16) Talukdar, K.; Issa, A.; Jurss, J. W. Synthesis of a Redox-Active NNP-Type Pincer Ligand and Its Application to Electrocatalytic CO2 Reduction with First-Row Transition Metal Complexes. *Front. Chem.* **2019**, 7, No. 330.
(17) Broere, D. L. J.; van Leest, N. P.; de Bruin, B.; Siegler, M. A.; van der Vlugt, J. I. Reversible Redox Chemistry and Catalytic C (Sp3)–H Amination Reactivity of a Paramagnetic Pd Complex Bearing a Redox-Active o-Aminophenol-Derived NNO Pincer Ligand. *Inorg. Chem.* **2016**, 55 (17), 8603−8611.
(18) Broere, D. L. J.; Metz, L. L.; de Bruin, B.; Reek, J. N. H.; Siegler, M. A.; van der Vlugt, J. I. Redox-Active Ligand-Induced Homolytic Bond Activation. *Angew. Chem. Int. Ed.* **2015**, 54 (5), 1516−1520.
(19) Kaim, W. *The Shrinking World of Innocent Ligands: Conventional and Non-Conventional Redox-Active Ligands*; Wiley Online Library, 2012.
(20) Das, A.; Ren, Y.; Hessin, C.; Desage-El Murr, M. Copper Catalysis with Redox-Active Ligands. *Beilstein J. Org. Chem.* **2020**, 16 (1), 858−870.

(21) Heyduk, A. F.; Zarkesh, R. A.; Nguyen, A. I. Designing Catalysts for Nitrene Transfer Using Early Transition Metals and Redox-Active Ligands. *Inorg. Chem.* **2011**, *50* (20), 9849−9863.

(22) Anderson, W. C., Jr; Rhinehart, J. L.; Tennyson, A. G.; Long, B. K. Redox-Active Ligands: An Advanced Tool to Modulate Poly-ethylene Microstructure. *J. Am. Chem. Soc.* **2016**, *138* (3), 774−777.

(23) Praneeth, V. K. K.; Ringenberg, M. R.; Ward, T. R. Redox-Active Ligands in Catalysis. *Angew. Chem., Int. Ed.* **2012**, *51* (41), 10228−10234.

(24) Ding, B.; Solomon, M. B.; Leong, C. F.; D'Alessandro, D. M. Redox-Active Ligands: Recent Advances towards Their Incorporation into Coordination Polymers and Metal-Organic Frameworks. *Coord. Chem. Rev.* **2021**, *439*, No. 213891.

(25) van der Vlugt, J. I. Radical-Type Reactivity and Catalysis by Single-Electron Transfer to or from Redox-Active Ligands. *Chem. - Eur. J.* **2019**, *25* (11), 2651−2662.

(26) Waltman, A. W.; Grubbs, R. H. A New Class of Chelating N-Heterocyclic Carbene Ligands and Their Complexes with Palladium. *Organometallics* **2004**, *23* (13), 3105−3107.

(27) Borré, E.; Dahm, G.; Aliprandi, A.; Mauro, M.; Dagorne, S.; Bellemin-Laponnaz, S. Tridentate Complexes of Group 10 Bearing Bis-Aryloxide N-Heterocyclic Carbene Ligands: Synthesis, Structural, Spectroscopic, and Computational Characterization. *Organometallics* **2014**, *33* (17), 4374−4384.

(28) Aihara, H.; Matsuo, T.; Kawaguchi, H. Titanium N-Heterocyclic Carbene Complexes Incorporating an Imidazolium-Linked Bis(Phenol). *Chem. Commun.* **2003**, No. 17, 2204−2205.

(29) Dagorne, S.; Bellemin-Laponnaz, S.; Romain, C. Neutral and Cationic N-Heterocyclic Carbene Zirconium and Hafnium Benzyl Complexes: Highly Regioselective Oligomerization of 1-Hexene with a Preference for Trimer Formation. *Organometallics* **2013**, *32* (9), 2736−2743.

(30) Romain, C.; Choua, S.; Collin, J.-P.; Heinrich, M.; Bailly, C.; Karmazin-Brelot, L.; Bellemin-Laponnaz, S.; Dagorne, S. Redox and Luminescent Properties of Robust and Air-Stable N-Heterocyclic Carbene Group 4 Metal Complexes. *Inorg. Chem.* **2014**, *53* (14), 7371−7376.

(31) Romain, C.; Fliedel, C.; Bellemin-Laponnaz, S.; Dagorne, S. NHC Bis-Phenolate Aluminum Chelates: Synthesis, Structure, and Use in Lactide and Trimethylene Carbonate Polymerization. *Organometallics* **2014**, *33* (20), 5730−5739.

(32) Weinberg, D. R.; Hazari, N.; Labinger, J. A.; Bercaw, J. E. Iridium(I) and Iridium(III) Complexes Supported by a Diphenolate Imidazolyl-Carbene Ligand. *Organometallics* **2010**, *29* (1), 89−100.

(33) Bellemin-Laponnaz, S.; Welter, R.; Brelot, L.; Dagorne, S. Synthesis and Structure of V (V) and Mn (III) NHC Complexes Supported by a Tridentate Bis-Aryloxide-N-Heterocyclic Carbene Ligand. *J. Organomet. Chem.* **2009**, *694* (5), 604−606.

(34) Min, K. S.; Weyhermüller, T.; Bothe, E.; Wieghardt, K. Tetradentate bis(o-iminobenzosemiquinonate(1-)) pi radical ligands and their o-aminophenolate(1-) derivatives in complexes of nickel(II), palladium(II), and copper(II). *Inorg. Chem.* **2004**, *43*, 2922−2931, DOI: 10.1021/ic0302480.

(35) Wang, D.; Astruc, D. The Golden Age of Transfer Hydrogenation. *Chem. Rev.* **2015**, *115* (13), 6621−6686.

(36) Brieger, G.; Nestrick, T. J. Catalytic Transfer Hydrogenation. *Chem. Rev.* **1974**, *74* (5), 567−580.

(37) Sluijter, S. N.; Korstanje, T. J.; van der Vlugt, J. I.; Elsevier, C. J. Mechanistic Insights into Catalytic Carboxylic Ester Hydrogenation with Cooperative Ru(II)-Bis{1,2,3-Triazolylidene}pyridine Pincer Complexes. *J. Organomet. Chem.* **2017**, *845*, 30−37.

(38) Wu, X.; Liu, J.; Di Tommaso, D.; Iggo, J. A.; Catlow, C. R. A.; Bacsa, J.; Xiao, J. A Multilateral Mechanistic Study into Asymmetric Transfer Hydrogenation in Water. *Chem. - Eur. J.* **2008**, *14* (25), 7699−7715.

(39) Albrecht, M.; Crabtree, R. H.; Mata, J.; Peris, E. Chelating Bis-Carbene Rhodium(Iii) Complexes in Transfer Hydrogenation of Ketones and Imines. *Chem. Commun.* **2002**, No. 1, 32−33. No.

(40) Enthaler, S.; Jackstell, R.; Hagemann, B.; Junge, K.; Erre, G.; Beller, M. Efficient Transfer Hydrogenation of Ketones in the Presence of Ruthenium N-Heterocyclic Carbene Catalysts. *J. Organomet. Chem.* **2006**, *691* (22), 4652−4659.

(41) Nie, R.; Tao, Y.; Nie, Y.; Lu, T.; Wang, J.; Zhang, Y.; Lu, X.; Xu, C. C. Recent Advances in Catalytic Transfer Hydrogenation with Formic Acid over Heterogeneous Transition Metal Catalysts. *ACS Catal.* **2021**, *11* (3), 1071−1095.

(42) Fernández, F. E.; Puerta, M. C.; Valerga, P. Ruthenium(II) Picolyl-NHC Complexes: Synthesis, Characterization, and Catalytic Activity in Amine N-Alkylation and Transfer Hydrogenation Reactions. *Organometallics* **2012**, *31* (19), 6868−6879.

(43) Monney, A.; Venkatachalam, G.; Albrecht, M. Synthesis and Catalytic Activity of Histidine-Based NHC Ruthenium Complexes. *Dalton Trans.* **2011**, *40* (12), 2716−2719.

(44) Pàmies, O.; Bäckvall, J.-E. Studies on the Mechanism of Metal-Catalyzed Hydrogen Transfer from Alcohols to Ketones. *Chem. - Eur. J.* **2001**, *7* (23), 5052−5058.

(45) Albrecht, M.; Miecznikowski, J. R.; Samuel, A.; Faller, J. W.; Crabtree, R. H. Chelated Iridium(III) Bis-Carbene Complexes as Air-Stable Catalysts for Transfer Hydrogenation. *Organometallics* **2002**, *21* (17), 3596−3604.

(46) Wei, Y.; Wu, X.; Wang, C.; Xiao, J. Transfer Hydrogenation in Aqueous Media. *Catal. Today* **2015**, *247*, 104−116.

(47) Ghosh, R.; Jana, N. C.; Panda, S.; Bagh, B. Transfer Hydrogenation of Aldehydes and Ketones in Air with Methanol and Ethanol by an Air-Stable Ruthenium−Triazole Complex. *ACS Sustainable Chem. Eng.* **2021**, *9* (13), 4903−4914.

(48) Witt, J.; Pöthig, A.; Kühn, F. E.; Baratta, W. Abnormal N-Heterocyclic Carbene-Phosphine Ruthenium(II) Complexes as Active Catalysts for Transfer Hydrogenation. *Organometallics* **2013**, *32* (15), 4042−4045.

(49) Clapham, S. E.; Hadzovic, A.; Morris, R. H. Mechanisms of the H2-Hydrogenation and Transfer Hydrogenation of Polar Bonds Catalyzed by Ruthenium Hydride Complexes. *Coord. Chem. Rev.* **2004**, *248* (21), 2201−2237.

(50) Dragutan, V.; Dragutan, I.; Delaude, L.; Demonceau, A. NHC−Ru Complexes—Friendly Catalytic Tools for Manifold Chemical Transformations. *Coord. Chem. Rev.* **2007**, *251* (5), 765−794.

(51) Bauer, I.; Knölker, H.-J. Iron Catalysis in Organic Synthesis. *Chem. Rev.* **2015**, *115* (9), 3170−3387.

(52) Fürstner, A. Iron Catalysis in Organic Synthesis: A Critical Assessment of What It Takes To Make This Base Metal a Multitasking Champion. *ACS Cent. Sci.* **2016**, *2* (11), 778−789.

(53) Wei, D.; Darcel, C. Iron Catalysis in Reduction and Hydrometalation Reactions. *Chem. Rev.* **2019**, *119* (4), 2550−2610.

(54) Hashimoto, T.; Urban, S.; Hoshino, R.; Ohki, Y.; Tatsumi, K.; Glorius, F. Synthesis of Bis(N-Heterocyclic Carbene) Complexes of Iron(II) and Their Application in Hydrosilylation and Transfer Hydrogenation. *Organometallics* **2012**, *31* (12), 4474−4479. (and references 5−67 therein).

(55) Zhao, N.; Hou, G.; Deng, X.; Zi, G.; Walter, M. D. Group 4 Metal Complexes with New Chiral Pincer NHC-Ligands: Synthesis, Structure and Catalytic Activity. *Dalton Trans.* **2014**, *43* (22), 8261−8272, DOI: 10.1039/C4DT00510D.

(56) Zhang, M.; Ni, X.; Shen, Z. Synthesis of Bimetallic Bis(Phenolate) N-Heterocyclic Carbene Lanthanide Complexes and Their Applications in the Ring-Opening Polymerization of l-Lactide. *Organometallics* **2014**, *33* (23), 6861−6867.

(57) Xia, C.-L.; Xie, C.-F.; Wu, Y.-F.; Sun, H.-M.; Shen, Q.; Zhang, Y. Efficient Cross-Coupling of Aryl Grignard Reagents with Alkyl Halides by Recyclable Ionic Iron(Iii) Complexes Bearing a Bis-(Phenol)-Functionalized Benzimidazolium Cation. *Org. Biomol. Chem.* **2013**, *11* (46), 8135−8144.

(58) Duguet, N.; Smith, A. D.; et al. Chiral Relay in NHC-Mediated Asymmetric β-Lactam Synthesis I; Substituent Effects in NHCs Derived from (1R,2R)-Cyclohexane-1,2-Diamine. *Tetrahedron: Asymmetry* **2010**, *21* (5), 582−600.

(59) Groysman, S.; Sergeeva, E.; Goldberg, I.; Kol, M. Salophan Complexes of Group IV Metals. *Eur. J. Inorg. Chem.* **2005**, *2005* (12), 2480−2485.

(60) Neshat, A.; Kakavand, M.; Osanlou, F.; Mastrorilli, P.; Schingaro, E.; Mesto, E.; Todisco, S. Alcohol Oxidations by Schiff Base Manganese(III) Complexes. *Eur. J. Inorg. Chem.* **2020**, *2020* (5), 480.

(61) Neshat, A.; Osanlou, F.; Kakavand, M.; Mastrorilli, P.; Schingaro, E.; Mesto, E.; Todisco, S. Catalytic Alcohol Oxidation Using Cationic Schiff Base ManganeseIII Complexes with Flexible Diamino Bridge. *Polyhedron* **2021**, *193*, No. 114873.

(62) Balamurugan, M.; Suresh, E.; Palaniandavar, M. μ-Oxo-Bridged Diiron(Iii) Complexes of Tripodal 4N Ligands as Catalysts for Alkane Hydroxylation Reaction Using m-CPBA as an Oxidant: Substrate vs. Self Hydroxylation. *RSC Adv.* **2021**, *11* (35), 21514−21526.

(63) Lator, A.; Gaillard, S.; Poater, A.; Renaud, J.-L. Well-Defined Phosphine-Free Iron-Catalyzed N-Ethylation and N-Methylation of Amines with Ethanol and Methanol. *Org. Lett.* **2018**, *20*, 5985−5990.

(64) Nugent, W. A.; Mayer, J. M. *Metal-Ligand Multiple Bonds*; John Wiley & Sons: New York, 1988.

(65) Holm, R. H. Metal-Centered Oxygen Atom Transfer Reactions. *Chem. Rev.* **1987**, *87* (6), 1401−1449.

(66) Hausinger, R. P. Fe(II)/α-Ketoglutarate-Dependent Hydroxylases and Related Enzymes. *Crit. Rev. Biochem. Mol. Biol.* **2004**, *39* (1), 21−68.

(67) Ortiz de Montellano, P. R. Hydrocarbon Hydroxylation by Cytochrome P450 Enzymes. *Chem. Rev.* **2010**, *110* (2), 932−948.

(68) Vaz, A. D. N.; McGinnity, D. F.; Coon, M. J. Epoxidation of Olefins by Cytochrome P450: Evidence from Site-Specific Mutagenesis for Hydroperoxo-Iron as an Electrophilic Oxidant. *Proc. Natl. Acad. Sci. U.S.A.* **1998**, *95* (7), 3555−3560.

(69) Farinas, E. T.; Alcalde, M.; Arnold, F. Alkene Epoxidation Catalyzed by Cytochrome P450 BM-3 139−3. *Tetrahedron* **2004**, *60* (3), 525−528.

(70) Korzekwa, K.; Trager, W.; Gouterman, M.; Spangler, D.; Loew, G. Cytochrome P450 Mediated Aromatic Oxidation: A Theoretical Study. *J. Am. Chem. Soc.* **1985**, *107* (14), 4273−4279.

(71) Brunold, T. C. Synthetic Iron-Oxo "Diamond Core" Mimics Structure of Key Intermediate in Methane Monooxygenase Catalytic Cycle. *Proc. Natl. Acad. Sci. U.S.A.* **2007**, *104* (52), 20641−20642.

(72) Schotten, C.; Bourne, R. A.; Kapur, N.; Nguyen, B. N.; Willans, C. E. Electrochemical Generation of N-Heterocyclic Carbenes for Use in Synthesis and Catalysis. *Adv. Synth. Catal.* **2021**, *363*, 3189−3200.

(73) Enders, D.; Breuer, K.; Raabe, G.; Simonet, J.; Ghanimi, A.; Stegmann, H. B.; Teles, J. H. A stable carbene as π-acceptor electrochemical reduction to the radical anion. *Tetrahedron Lett.* **1997**, *38*, 2833−2836.

(74) Harris, C. F.; Bayless, M. B.; van Leest, N. P.; Bruch, Q. J.; Livesay, B. N.; Bacsa, J.; Hardcastle, K. I.; Shores, M. P.; de Bruin, B.; Soper, J. D. Redox-Active Bis(phenolate) N-Heterocyclic Carbene [OCO] Pincer Ligands Support Cobalt Electron Transfer Series Spanning Four Oxidation States. *Inorg. Chem.* **2017**, *56*, 12421−12435.

(75) Tsui, B. T. H.; Sung, M. M. H.; Kinas, J.; Hahn, F. E.; Morris, R. H. A Ruthenium Protic N-Heterocyclic Carbene Complex as a Precatalyst for the Efficient Transfer Hydrogenation of Aryl Ketones. *Organometallics* **2022**, *41*, 2095−2105. (and references 37 41 61 71,−73 therein)

(76) Palatinus, L.; Chapuis, G. SUPERFLIP− a computer program for the solution of crystal structures by charge flipping in arbitrary dimensions. *J. Appl. Crystallogr.* **2007**, *40* (4), 786−790.

(77) Petříček, V.; Dušek, M.; Palatinus, L. Crystallographic Computing System JANA2006: General features. *Z. Kristallogr. - Cryst. Mater.* **2014**, *229* (5), 345−352.

(78) Betteridge, P. W.; Carruthers, J. R.; Cooper, R. I.; Prout, K.; Watkin, D. J. Software for guided crystal structure analysis. *J. Appl. Crystallogr.* **2003**, *36*, 1487.

(79) Macrae, C. F.; Sovago, I.; Cottrell, S. J.; Galek, P. T. A.; McCabe, P.; Pidcock, E.; Platings, M.; Shields, G. P.; Stevens, J. S.; Towler, M.; Wood, P. A. Mercury 4.0: from visualization to analysis, design and prediction. *J. Appl. Crystallogr.* **2020**, *53*, 226−235.